

pubs.acs.org/JPCC Article

Exploring the A₂BX₃ Family for New Functional Materials Using Crystallographic Database Mining and First-Principles Calculations

Joseph W. Bennett*



Cite This: J. Phys. Chem. C 2020, 124, 19413-19425



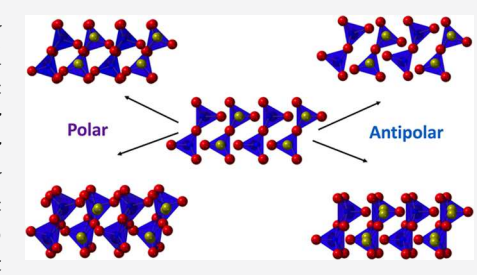
ACCESS I

III Metrics & More

Article Recommendations

Supporting Information

ABSTRACT: Ferroelectrics (FEs) are increasingly finding use as solar energy conversion materials. One of the hallmark signatures of a proper FE is a polar ground state whose polarization can be switched through an intermediate paraelectric nonpolar state. For a material to be considered as a candidate proper FE, their ground-state structure should be classified in a polar space group and/or a polar structure type and the barrier to polarization switching should not be prohibitively large. The Na₂SiO₃ structure type is polar, and the Inorganic Crystallographic Structure Database shows that some materials in this polar structure type have also been classified in other nonpolar structure types. Further investigation shows that these nonpolar structure types are themselves related to other antipolar structure



types, where the entries of interest share a common chemical formula of A_2BX_3 . Appearing in multiple structure types might be an indication that members of a material family can undergo phase transitions from nonpolar supergroups to polar and antipolar subgroups and be considered as candidate FEs or antiferroelectrics (AFEs). To the best of our knowledge, the literature shows no evidence of these materials demonstrating a switchable polarization, nor has there been any prior report on the symmetry relationships within this family. Here, we combine crystallographic database mining and first-principles density functional theory (DFT) calculations to first establish the symmetry relationships in a family of materials and then assess if any of the known members are potentially proper (or improper) FEs or AFEs. Finally, we provide qualitative guidance for future experimental endeavors aimed at creating new functional materials from the A_2BX_3 family.

■ INTRODUCTION

The last decade has witnessed a dramatic increase in publications devoted to materials by design, specifically the use of computation and data mining to study new materials before they are synthesized.^{1–4} Well-known successes in this field, where the results of computational modeling and synthetic advances have worked in tandem to create new materials, are hybrid perovskites as photovoltaics,^{5–8} complex chalcogenides as thermoelectrics,^{9–12} and compositionally tuned iron pnictides as superconductors.^{13,14} Many of these new materials have been made possible by scientists harnessing what has been coined "the data revolution"; the internet allows for rapid retrieval of previously inaccessible information, and progress in semiconductor technology, alongside the concurrent development of computer architectures and advanced algorithms, allows for a multitude of calculations that were previously daunting.

Combining information available through online databases with first-principles calculations, ^{15–17} in this case the Inorganic Crystal Structure Database (ICSD)¹⁸ and density functional theory (DFT) calculations, ^{19,20} has already led to critical insights into the design and discovery of new functional materials that exhibit previously unknown ranges of technologically relevant properties, ^{1,21–30} as well as the ability to relate those properties to structural features and create novel multifunctional materials. ^{31–40} We can use the crystallographic information in the ICSD to search for similar and/or related

materials, group them into families called structure types, ⁴¹ and use each database entry as the input for DFT calculations. This is because each entry in the ICSD is a compound that has been previously characterized and documented, so there is specific crystallographic information such as the space group designation, lattice constants, Wyckoff parameters, and coordinates for each atom in the structure. These calculations can determine if a member of the structure type exhibits any functional property that may have been previously overlooked. Various search strategies for crystallographic database mining can be found in refs 15–17, 42, and 43 and examples where this strategy has yielded new families of functional materials include the half-Heusler family as piezoelectrics, ⁴⁴ the LiGaGe structure type as ferroelectrics (FEs), ^{45–47} and the MgSrSi structure type as antiferroelectrics (AFEs). ⁴⁸

The combination of database mining and DFT calculations is well-suited in the search for new FEs and AFEs that can be used as materials for energy generation (FEs) and energy storage

Received: April 7, 2020 Revised: August 4, 2020 Published: August 12, 2020





(AFEs). ^{49–54} Proper ferroelectrics have a polar ground-state structure whose polarization can be switched (most times by an external electric field) via a higher-symmetry nonpolar paraelectric intermediate state. ^{45,55} The polar ground states can be described as symmetry-related distortions of the paraelectric intermediate state, where the primary structural distortion is a zone center polar mode. Switching between these states can often be described as continuous (second order) phase transitions, exemplified by the polar Γ modes that relates the cubic and tetragonal phases of PbTiO₃, BaTiO₃, and complex perovskite superlattices. ^{55–58} Antiferroelectric materials require two criteria to be met. First, they must have an antipolar ground-state structure (with net P=0) that can be switched into polar states, and second, they need to be close in energy to a FE state. ⁵⁹ This implies that to find new AFEs we may need to find new example FEs.

One can search for new proper FEs by finding known materials in a polar space group, symmetry-related nonpolar structures, and finally, use DFT to compute both the polarization and estimated barriers to switching between them. The barrier to switching is approximated as ΔE , which is the difference in total energy between the polar and nonpolar structures. A small ΔE is an indication of whether a polar material is likely to be switchable. The DFT-computed ΔE of the known FE oxides BaTiO₃ and PbTiO₃ are ≈0.02 and 0.2 eV/ f.u., 55 where the larger ΔE value has been chosen as an upper limit or maximum threshold for potential switching in prior work. 17,45 This metric is a qualitative approximation intended to reduce the total number of candidate FEs that result from a DFT-based search. Employing a maximum barrier to switching creates smaller sets of materials to explore within a family. This enables targeted sets of future experimental endeavors, focusing on materials that (i) may already fit textbook definitions of the functional properties but have previously been unexplored or (ii) require fine tuning of the experimental parameters such as atomistic composition or epitaxial strain to adjust phase transition enthalpies and induce specific responses. The DFTcomputed energy difference underestimates the energy required to switch states in laboratory-synthesized FE materials, since switching between the polar and paraelectric states in actual materials proceeds through complex processes, such as domain wall nucleation (not taken into account here), and is dependent upon characteristics of the synthesized materials, such as thickness and vacancy composition. 17,32,48,59,

The search for new FEs and AFEs might not require starting from scratch; examples may already exist in a set of known materials that have already been synthesized and characterized, but previously overlooked as candidate FEs and AFEs. ^{17,45,48,60} Here, we use a combination of first-principles DFT and database mining to explore the structure—property relationships of known oxides and chalcogenides as materials with energy applications. We focus on the symmetry relations discussed in the previous paragraphs, which to the best of our knowledge is the first systematic symmetry analysis applied to this set of materials. The oxides and chalcogenides studied here distributed across four known structure types and can be formed through a variety of synthetic routes that include sol—gel syntheses, molten hydroxide flux, substitution reactions, and hydrothermal growth, ^{61–65} making them attractive from a synthetic point of view as well.

We screen 18 different known combinations of elements that are found in the ICSD across four known structure types, which are (a) the nonpolar orthorhombic $CsCu_2Cl_3$ type, (b) the

antipolar orthorhombic K_2SnO_3 type, (c) the polar orthorhombic Na_2SiO_3 type, and (d) the antipolar monoclinic Na_2CS_3 type. Our analysis determines that the polar Na_2SiO_3 type cannot be a proper FE structure type for materials of the chemical formula $A_2^{1+}B^{4+}X_3^{2-}$, so we instead present routes to potentially stabilize candidate FEs in symmetry-related polar structures. Our investigation maps out the phase space of the known materials, including relative energetics and the barriers to switch between states, and finally, we go on to compute the polarization, effective charge, and dielectric constant (where appropriate) to assess the properties of the family. This information is then used to inform future design strategies aimed at creating FEs and AFEs from the members of this family.

METHODOLOGY

Database Mining and Establishing Crystallographic Relationships. Guided by previous studies on the classification of polar structure types, 16,43 we find that the Na₂SiO₃ family of materials of $Cmc2_1$ symmetry (space group 36, polar) contains (i) more than 50 total entries in the ICSD, (ii) a range of cation combinations (A¹⁺ = Li, Na, K, Rb, Cs, Ag, Cu, and B⁴⁺ = Ti, Si, Ge, Pb), and (iii) a range of group VI anions (X²⁻ = O, S). The set of materials from the Na₂SiO₃ structure type that we will include in our study have the general formula $A_2^{1+}B^{4+}X_3^{2-}$ and are Li₂SiO₃, Li₂GeO₃, Na₂SiO₃, Na₂GeO₃, K₂PbO₃, Rb₂PbO₃, Cs₂PbO₃, Cs₂TiS₃, Cu₂SiS₃, and Ag₂GeS₃.

Further scrutiny of the entries in the Na₂SiO₃ structure type shows that Cs₂PbO₃⁶⁶ is also reported in *Cmcm* (space group 63, nonpolar) symmetry, in the CsCu₂Cl₃ structure type.⁶⁷ While these two structure types appear unrelated, the CsCu₂Cl₃ type contains at least three different example stoichiometries of compounds with various oxidation states: Cs¹⁺Cu₂¹⁺Cl₃¹⁻, $Ba^{2+}Fe_2^{2+}S_3^{2-}$, and $Pb^{4+}Cs_2^{1+}O_3^{2-}$. The WYCKSPLIT program⁶⁸ (hosted at the Bilbao Crystallographic Server^{69,70}) shows that the Wyckoff sequence of space group 63 (gec2) can be related to subgroup 36 (b2a2) without cell doubling, but only a few members of the CsCu₂Cl₃ type can be related via a continuous distortion to the lower-symmetry Na₂SiO₃ structure type. These members have cation oxidation states of 1+ and 4+, where each cation is located at Wyckoff sites 8g and 4c, respectively. Entries in the CsCu₂Cl₃ structure type that adhere to this symmetry constraint are PbCs₂O₃, ZrCs₂O₃, TiK₂O₃, and ZrCs₂Se₃, which will be referred to here using the A₂¹⁺B⁴⁺X₃²⁻ formatting for easier comparison. We use the ISODISTORT program, 71 housed within the ISOTROPY software suite, 72 to find that the two structure types are related by a polar zone center mode, Γ^{2-} , which is one of the irreducible representations (irreps) of orthorhombic *Cmcm* symmetry.

A continuous second-order phase transition between members of the $CsCu_2Cl_3$ and Na_2SiO_3 structure types is possible; however, we will still need to compute ΔE to assess the likelihood of switchability. While a continuous second-order phase transition between high- (nonpolar) and low (polar)-symmetry exists for proper FEs such as $BaTiO_3$ and $PbTiO_3$, as well as the class of ABC hyperferroelectrics, it is not a necessary condition for all FE behavior. There exist classes of materials called improper FEs, where a nonzero polarization is induced with no zone center distortions (e.g., YMnO₃) and hybrid improper FEs, where multiple nonpolar structural distortions combine to break symmetry and allow for a nonzero polarization through trilinear mode coupling (e.g., $Ca_3Mn_2O_7$). S8,76,77 An advantage to hybrid improper FEs is that there are potentially multiple switching paths available that

do not need to include a high-symmetry paraelectric state. While the goal of the work presented here is to search for proper FEs and related AFEs using symmetry relationships and DFT calculations, this does not preclude the data generated from this study from being used to screen for additional types of improper FE behavior.

Two members of the $CsCu_2Cl_3$ structure type, $K_2PbO_3^{79}$ and $Rb_2PbO_3^{80}$ are also reported in *Pnma* symmetry (space group 62) in the K_2SnO_3 structure type. ^{67,81} The K_2SnO_3 structure type includes two more entries of similar chemical formula, K_2SnO_3 and K_2ZrO_3 , which will be included here. Figure 1

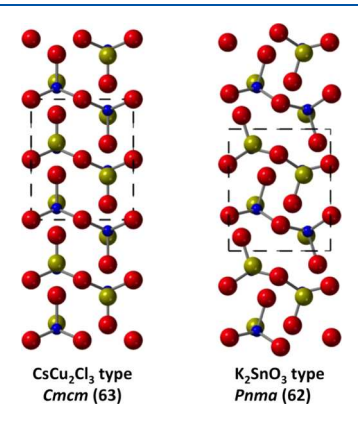


Figure 1. Compared here are the side views of the structure types found in orthorhombic symmetries *Cmcm* (space group 63) and *Pnma* (space group 62). The A-sites (Li, Na, K) are gold spheres, the B-sites (Si, Ge, Pb) are blue spheres, and the X-sites are red spheres (O, S, Se). The dashed black lines indicate the dimensions of the unit cell.

depicts the structural differences between the CsCu₂Cl₃ (space group 63) and K₂SnO₃ (space group 62) types. This figure highlights the antipolar displacements in Pnma symmetry that are absent in Cmcm symmetry; antipolar buckling of the A-sites is coupled to antipolar buckling of the edge-sharing BX5 pyramids. If the K₂SnO₃ type is antipolar, it may include AFEs whose functional properties have not yet been investigated. The Wyckoff sequence of group 63 (gec2) can be related to subgroup 62 (d2c2) using WYCKSPLIT, and a continuous antipolar distortion can be described using ISODISTORT to relate the CsCu₂Cl₃ and K₂SnO₃ structure types. This distortion mode is Y^{2-} , an irrep of *Cmcm* symmetry. Finally, another antipolar structure type that can be related to the CsCu₂Cl₃ structure type via continuous distortion, and contains entries of chemical formula $A_2^{1+}B^{4+}X_3^{2-}$, is Na_2CS_3 . 82 This structure type belongs in C2/c symmetry (space group 15) and contains two entries: Na₂CS₃ and Tl₂CS₃.⁶³ There is another entry in space group C2/ c, K₂TiS₃, 83 which is unassigned a structure type but fits into our Wyckoff sequence and chemical formula rules. The distortion mode that relates these two structure types is Γ^{4+} , an irrep of Cmcm symmetry.

From a materials design perspective, this range of structure types (polar Na_2SiO_3 , nonpolar $CsCu_2Cl_3$, and antipolar K_2PbO_3 and Na_2CS_3) are a family of potentially untapped multifunctional materials: the present work is the first investigation into the FE and AFE nature of the atomistic displacements that relate the structure types. Beyond the mappable phase transitions described in the last three paragraphs, the A-sites offer a wide range of crystallographic free parameters to encourage polar displacements, the B-site is reported to be either 3, 4, or 5-fold coordinate, depending upon

the pairing of different species, ^{63,82,83} and there are two crystallographically distinct anion X-sites. Taken together, this suggests that changes in the composition will result in selective displacement patterns, where additional symmetries can be stabilized, and warrants exploration of these families of structure types as materials that are capable of supporting ferroelectricity and/or antipolar displacements. This idea, combined with the fact that the dielectric and piezoelectric properties of some polar members (Li₂SiO₃, Li₂GeO₃, Na₂GeO₃) have been previously published, ^{84,83} as have vibrational spectra and multiple growth conditions, ^{65,86,87} could yield an easily synthesizable class of FEs and AFEs whose entire set of functional properties have previously gone overlooked.

DFT Modeling. The ground-state calculations presented here employ periodic DFT methods^{19,20} and are carried out using ABINIT, an open source software package. 88,89 All atoms are represented using optimized norm-conserving Vanderbilt (ONCV) pseudopotentials 90-92 and a plane-wave cutoff of 50 Ry. Bulk structural relaxations use a $6 \times 6 \times 3$ k-point grid, ⁹³ and the convergence criterion for self-consistent relaxations was 5 \times 10^{-6} eV. This criterion allows for ΔE comparisons down to at least 1 meV and also results in relaxed structures with maximum residual forces of $\approx 1-5$ meV/Å per atom. These stringently relaxed structures are taken on to density functional perturbation theory (DFPT) calculations, as implemented in ABINIT, to compute dynamical matrices, Born effective charges (Z^*) , and dielectric constants (ϵ) for representative bulk structures. 94,95 Where applicable, we report polarization using the Berry phase approach. 96,97 All calculations are performed at the generalized gradient approximation (GGA) level using the Wu-Cohen (WC)-modified Perdew-Burke-Ernzerhof (PBE)-GGA exchange-correlation functional for solids. 98,99 We choose the WC-modified PBE-GGA because of its (i) improved agreement with the experimental structures for a wide range of semiconductors, including oxides and chalcogenides, 100 (ii) ability to match well the properties of known FEs PbTiO₃ and BaTiO₃, ⁹⁹ and (iii) utility in investigating phase transitions of FEs, ¹⁰¹ even when compared to meta-GGA functionals. ¹⁰² To demonstrate the improvement in the DFT-computed properties of WC over PBE, we include in Section S4 of the Supporting Information a brief discussion and comparison of the lattice parameters and ΔE for select compositions.

■ RESULTS AND DISCUSSION

Atomic Displacement Mode Analysis. For the 18 A₂BX₃ compositions described above, inspection of the references given in the ICSD shows that there are potentially related stoichiometries and structure types. Cs₂ZrSe₃, Cs₂PbO₃, and Cs₂ZrO₃ (in the CsCu₂Cl₃ type) are referred to as related to Cs_2TiS_3 (in the Na_2SiO_3 type), Cs_2TiS_3 and Cs_2TiS_3 was referred to as related to Cs_2TiS_3 (not assigned a type), Cs_2TiS_3 but to the best of our knowledge, there has not yet been a systematic investigation of exactly how the different structure types are related, if at all. To investigate these relationships beyond the crystallographic speculations presented in refs 83, 103, and 104, we turn again to the ISOTROPY⁷² suite of programs, specifically ISODIS-TORT⁷¹ and ISOCIF. For our atomic displacement mode analysis, we create crystallographic input files using ISOCIF, another program in the ISOTROPY suite, based on the standardized crystallographic information presented in the ICSD: each 1+ cation is called A, each 4+ cation is called B, and each 2- anion is called X. This ensures that all known crystal structures have the same generic chemical formula $A_2^{1+}B^{4+}X_3^{2-}$,

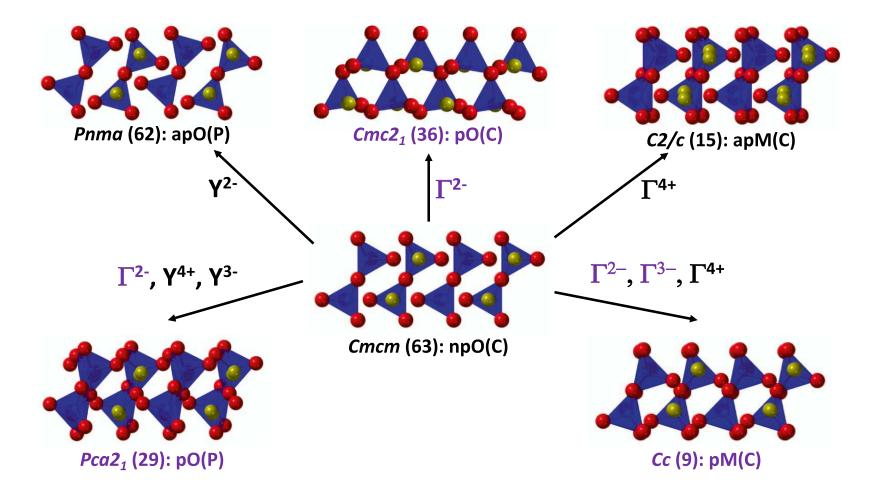


Figure 2. Distortion modes from high-symmetry reference structure type npO(C) can be used to describe the displacements to lower-symmetry subgroup structure types apO(P), pO(C), pO(P), apM(C), and apM(C). Polar structure types and irreps that correspond to polar modes are labeled in purple text and all others are in black text. The atomic color scheme is the same as before, except the BX_y polyhedra are shaded to show connectivity and changes in relative orientation.

and that the atomic distortion modes, generated using ISOTROPY, can be compared from a purely structural basis that is not influenced by atomistic identity across multiple compositions with different A, B, and X.

For ease of analysis and description, we will refer to each structure type with the following format: polarization state, crystal class, and the leading letter of the space group in parentheses. For example, the CsCu₂Cl₃ structure type is classified as nonpolar (np) and found in orthorhombic (O) Cmcm (C) space group 63: it is referred to as the npO(C) type. The K₂SnO₃ type in space group 62 (antipolar orthorhombic Pnma symmetry) will be called apO(P), the Na₂SiO₃ type in space group 36 (polar orthorhombic Cmc2, symmetry) will be called pO(C), and the Na₂CS₃ type in space group 15 (antipolar monoclinic C2/c symmetry) will be called apM(C). This means that apO(P), pO(C), and apM(C) will be considered subgroup structure types of the npO(C) group structure type, and that descriptions of atomistic displacement modes will be given with respect to npO(C). These modes are listed in Figure 2, yielding a great deal of information when combined with visualization of each structure type. All crystallographic information needed to reproduce our DFT-relaxed structures, including lattice parameters, Wyckoff positions, and origin translations, are given in Sections S1 and S2 of the Supporting Information.

The Γ^{1+} irrep is present in all of the symmetry analyses since it is the totally symmetric representation. This mode couples to changes in volume between the npO(C) and low-symmetry structure types and also yields insights into cell strains. What differentiates the lower-symmetry structure types from each other are the irreps that are not Γ^{1+} . Each irrep will be referred to as primary and secondary modes, where possible. Starting from the top left-hand side of Figure 2, from the high-symmetry npO(C) type to lower-symmetry apO(P) type, the primary distortion mode is the Y2- irrep that includes minor displacements of A and B cations along the x, y, and z directions and larger displacements of X anions along the x direction. The net effect is an antipolar structure. The primary distortion mode that describes the transition from npO(C) to pO(C) type is a polar Γ^{2-} irrep (top, middle of Figure 2), which includes sizable displacements of A, B, and C ions in the z direction. These displacements are large enough to alter the bond connectivity and change the coordination environment. Inducing this polar

displacement mode changes the edge-sharing BX_5 square pyramids into corner-sharing BX_4 tetrahedra. The net effect of inducing this distortion is a polar structure type where multiple bonds have been broken relative to the high-symmetry reference structure npO(C) type. An illustration of the computed change in coordinates and connectivity for this phase transition is shown in Figure 3. Inducing the primary displacement mode that can be

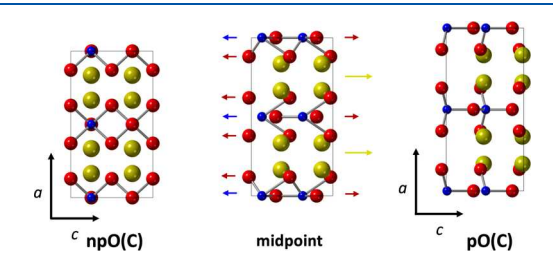


Figure 3. Depiction of the change from high-symmetry reference structure type $\operatorname{npO}(C)$ to lower-symmetry subgroup structure type $\operatorname{pO}(C)$ with an extrapolated midpoint. The atomic color scheme is the same as before, and the BX_y bonds that are \leq 2.2 Å show changes in connectivity over a proposed phase transition.

described as the Γ^{4+} irrep, one can induce a change from the npO(C) to apM(C) type (top right-hand side of Figure 2). This mode creates antipolar displacements of A in z, no net displacements of B, and antipolar displacements of X in y and z. The apM(C) type has $\beta > 90^{\circ}$, so the A and C atoms are no longer coincidental in Figure 2.

This analysis shows that apO(P) and apM(C) types can be considered antipolar subgroups of the npO(C) type, and as shown in Figure 2, that the induced displacements are easily mappable when compared to the transition between the npO(C) and pO(C) types. The pO(C) structure type involves too much reorganization to be considered a ferroelectric subgroup of npO(C); Figure 3 shows how radically altered the atoms become over the proposed second-order phase transition. The biggest changes are (i) the lattice constant a in most cases is 2-3 Å larger than the comparable stoichiometries in the pO(C) type and (ii) the npO(C) type contains five B-X bonds and the pO(C) type contains four B-X bonds. These changes can be rationalized by the displacement patterns depicted in Figure 3: the A atoms (gold spheres) shift to the

Table 1. Tabulated Here are the Ground-State Structure Type (ST_{gs}) and Then the Structure Type That is Energetically Closest to the Ground State, Which We Term Metastable (ST_{ms}) for Each A_2BX_3 Composition^a

material	ST_{gs}	а	ь	с	β	ST_{ms}	а	ь	с	β	ΔE
		(Å)	(Å)	(Å)			(Å)	(Å)	(Å)		(meV)
Na ₂ CS ₃	apM(C)	9.917	6.297	8.504	107.9	apO(P)	7.312	11.083	6.607	90.0	124
Tl_2CS_3	apM(C)	10.884	6.447	9.114	117.8	apO(P)	7.139	9.997	8.028	90.0	30
Li_2SiO_3	pO(C)	9.422	5.409	4.652	90.0	pM(C)	9.297	5.453	5.418	121.9	132
Na ₂ SiO ₃	pO(C)	10.479	6.132	4.868	90.0	pO(P)	6.226	8.894	4.967	90.0	557
Li_2GeO_3	pO(C)	9.663	5.508	4.874	90.0	apM(C)	9.205	5.820	5.263	120.1	114
Na ₂ GeO ₃	pO(C)	10.852	6.233	4.960	90.0	pO(P)	6.299	9.130	5.267	90.0	330
K_2SnO_3	apO(P)	5.815	10.380	6.987	90.0	pO(C)	10.412	6.995	5.806	90.0	6
K_2PbO_3	apO(P)	6.043	10.603	6.924	90.0	pO(C)	10.657	6.935	6.027	90.0	3
Rb ₂ PbO ₃	apO(P)	6.082	10.925	7.316	90.0	pO(C)	10.970	7.322	6.075	90.0	3
Cs ₂ PbO ₃	pM(C)	11.316	7.709	6.110	90.0	apO(P)	6.113	11.297	7.712	90.0	2
Cu_2SiS_3	pO(C)	10.715	6.298	6.053	90.0	apO(P)	5.839	9.662	6.463	90.0	529
Ag_2GeS_3	pO(C)	11.655	6.929	6.455	90.0	apO(P)	6.145	10.499	7.092	90.0	181
K_2ZrO_3	apO(P)	5.866	10.415	6.925	90.0	pO(P)	6.931	10.454	5.851	90.0	6
K_2TiS_3	apO(P)	6.446	11.748	8.227	90.0	apM(C)	11.698	8.279	6.433	93.4	5
K_2TiO_3	npO(P)	10.068	6.868	5.450	90.0	npO(C)	10.029	6.913	5.443	90.0	1
Cs_2TiS_3	npO(C)	12.474	8.943	6.459	90.0						
Cs_2ZrO_3	npO(C)	11.206	7.617	5.914	90.0						
Cs ₂ ZrSe ₃	npO(C)	13.008	9.371	7.084	90.0	apM(C)	13.090	9.297	7.085	90.0	1

"Listed for each entry, for the ground state (gs) and metastable state (ms), are the structure types, followed by the lattice parameters a, b, c, β , where lattice constants are given in units of angstrom. The final column is the difference in total energy per formula unit (ΔE) between the ground-state and lowest-energy metastable structure types, in units of millielectronvolt.

right along c as the B atoms (blue spheres) shift to the left, also along c, and as this happens, the X atoms (red spheres) also show two different sublattice shifts. The X atoms bound to B (along b, pointing into the plane of the figure) displace to the right and the X atoms closest to the A atoms left. Representative B—X bond lengths for the npO(C) and pO(C) types are 1.90 and (4×)2.08 Å and (2×)1.93 and (2×) 2.02 Å, respectively. The extrapolated midpoint in Figure 3 is generated to guide the eye to the changes that occur as the structure reorganizes and is not a structure type investigated here. The pO(C) type will not be a proper ferroelectric if the high-symmetry reference type is npO(C): the primary polar mode Γ^{2-} is too large, creating structural displacements that are unlikely to be switched.

One can use additional features of the ISOTROPY suite to ascertain if the primary polar distortion mode, Γ^{2-} , can be coupled to secondary distortions by searching for related symmetries. As shown in the bottom half of Figure 2, Γ^{2-} will couple with additional displacement modes, and the resulting structures can be described as two new structure types: pO(P) and pM(C). They are found in polar orthorhombic $Pca2_1$ (space group 29) symmetry and polar monoclinic Cc (space group 9) symmetry, respectively, and both pO(P) and pM(C) will be included in our DFT calculations. To obtain the pO(P) and pM(C) types, one needs to induce distortions that can be described as multiple irreps of Cmcm symmetry.

There are a multitude of ways to combine two or more atomistic displacements to create new polar structure types that could be classified as proper or improper ferroelectrics. Here, we choose two to create the pO(P) and pM(C) types. For the pO(P) type, inducing displacements that can be described using only the primary Y⁴⁺ mode will yield a structure of nonpolar *Pbcn* (60) symmetry, and inducing only the primary Y³⁻ irrep will yield nonpolar *Pbcm* (57) symmetry. Coupling these irreps will yield a structure of polar $Pca2_1$ (29) symmetry, in which the polar Γ^{2-} distortion acts as a secondary distortion mode.

Stabilizing this new structure type could result in a route to new examples of hybrid improper ferroelectric that do not include octahedral rotations. In the new pO(P) type, the atomic displacements previously observed in the pO(C) type are present along the c axis, but hindered enough that the pO(P) type maintains the edge-sharing BX₅ square-pyramidal geometry observed in the high-symmetry npO(C) structure type. The same type of description can be used to understand the new pM(C) type. It is a combination of primary displacement modes that can be described as using the Γ^{4+} irrep, which previously gave the apM(C) type, and the Γ^{2-} irrep. Inducing both of these displacement modes results in a new structure type of polar Cc (9) symmetry. If this type could be stabilized, the pM(C) type would be a new example proper ferroelectric. This structure type can also allow for a polar Γ^{3-} irrep (which induced by itself would yield a structure of Ama2 (40) symmetry) to act as a secondary distortion mode, that if stabilized would be an example of an improper ferroelectric coupling.

Taken altogether, our symmetry analysis sheds light on the structure—property relationships of the ${\rm A_2}^{1+}{\rm B}^{4+}{\rm X_3}^{2-}$ family of materials. We show why the polar ${\rm Na_2SiO_3}$ has not previously demonstrated a ferroelectric effect in experiments and use the results of this symmetry analysis to postulate the existence of multiple polar and antipolar structure types of orthorhombic or monoclinic crystal symmetry that can be classified as proper or hybrid improper ferroelectrics. In conjunction with DFT calculations of relaxed structures of related structure types, this type of symmetry analysis can be used to map out the potential energy landscape of a family of unexplored, but readily synthesizable materials.

Analysis of DFT Relaxations. We compute the relaxed structures of 18 A_2BX_3 combinations across the six structure types discussed in the previous section. These are the npO(C), apO(P), pO(C), pO(P), apM(C), and pM(C) types and are depicted in Figure 2, where the high-symmetry npO(C) type can be related via continuous displacements to all five lower-

symmetry structures types. All input structures for DFT calculations of the apO(P), pO(C), pO(P), apM(C), and pM(C) type are created by inducing symmetry breaking distortions from the npO(C) type that are consistent with each subgroup type. Each of these calculations is initialized with the atomic displacement patterns that contain the irreps of the npO(C) type, that appear in Figure 2, and are let fully relax. For the calculations presented here, we found that the structures either relaxed in and maintained the symmetry of the structure type it was initialized in or the structure relaxed into a higher-symmetry structure type. The latter is common in structures where the induced atomic displacements are not stable. The complete set of DFT-relaxed lattice parameters for all 18 combinations appears in Section S1 of the Supporting Information.

Inspection of the tabulated data in Table 1 gives insights into how cation pairings will result in a set of most likely ground-state structures. If a late (d^{10}) transition metal is paired with the main group elements that preferentially form tetrahedra (Si and Ge), then the combination will yield a pO(C) structure type as its ground state. These are the compositions Cu₂SiS₃ and Ag₂GeS₃. If an early (d⁰) transition metal is paired with an alkali cation, then the combination will yield ground-state structures that are either the npO(C) or apO(P) type. The compositions that relax to the npO(C) type are Cs₂TiS₃, Cs₂ZrO₃, and Cs₂ZrSe₃, and the compositions that relax to the apO(P) type are K_2TiO_3 , K_2TiS_3 , and K2ZrO3. It should be noted that there are three discrepancies between our DFT-computed ground-state structure and what is reported in the ICSD. K₂TiS₃ is reported in the ICSD in the apM(C) type 83 and Cs_2TiS_3 is reported in the pO(C) type, 107 while our DFT ground states are the apO(P) and npO(C) types, respectively. Finally, K2TiO3 is reported in the npO(C) type, which we compute is 1 meV/f.u. higher then our computed apO(P) ground state. These discrepancies are discussed in more detail in Section S3 of the Supporting Information.

If a main group element (alkali or Tl¹⁺ cations) is paired with another main group element, then they will yield a ground-state structure type that is apM(C), pO(C), or apO(P). This assignment appears to be dictated by the size and preferred coordination of the B-site: if it is a 3-fold coordinate C, it relaxes to a ground-state apM(C) type, whereas Si and Ge are 4-fold coordinate and relax to pO(C)-type ground states, while Sn and Pb are 5-fold coordinate and relax to apO(P) type. The compositions whose ground states are the apM(C) type are Na₂CS₃ and Tl₂CS₃, while Li₂SiO₃, Li₂GeO₃, Na₂SiO₃, and Na₂GeO₃ are found in the pO(C) type, and K₂SnO₃, K₂PbO₃, and Rb₂PbO₃ relax to ground states of type apO(P). Our only outlier from the trends listed above is Cs₂PbO₃, for which we obtain a pM(C) type ground state, but it is only 3 meV/f.u. lower in total energy than any of the other five structure types. A discrepancy exists in the ICSD for this composition as well. Cs_2PbO_3 has been identified in both the $npO(C)^{67}$ and $pO(C)^{66}$ types. Given that Cs and Pb both have large Z, this might be a material to revisit with a higher level theory (meta-GGA SCAN functional 102,108,109) that includes spin-orbit coupling as well as more rigorous, temperature-controlled experimental characterization. Including neutron refinement in addition to low-temperature X-ray diffraction studies could be a useful comparison to refs 67 and 66, elucidating if entropic effects were responsible for the multiple structure type assignments.

We classify the 18 compositions in Table 1 by DFT-calculated ground state and then go on to compare their metastable state that is lowest in total energy. The complete set of all DFTcomputed structures are reported in Section S1 of the Supporting Information. Here, we focus our discussion on the DFT-computed ground-state structure types and the structure type closest in total energy to assess the likelihood of switchability. For a combination to be a proper FE, it must have a polar ground-state structure type (pO(C), pO(P),pM(C)) and demonstrate switchability by having ΔE with a nonpolar type (npO(C)) below 200 meV/f.u. For a combination to be antiferroelectric, it must have an antipolar ground state (apO(P), apM(C)) and be energetically close to a FE. For any of our compositions to have an additional improper contribution to the FE polarization, they must either have (i) a pO(P) type ground state that includes a nonzero Γ^{2-} contribution or (ii) a pM(C) type ground state that includes a nonzero Γ^{3-} contribution. All DFT-computed lattice parameters and ΔE are reported in Tables S1-S3 of the Supporting Information.

Two of the 18 compositions are found only in the npO(C)type: Cs₂TiS₃, and Cs₂ZrO₃. Cs₂TiS₃ is in disagreement with the prior experimental studies, as it was reported in the pO(C) type. 107 For these combinations, no polar displacements were stable: all structures initialized with atomic displacement patterns that contained the Γ^{2-} irrep of the npO(C) type (which are the pO(C), pO(P), and pM(C) types) relaxed to the higher-symmetry npO(C) type. We also compute that a third composition, Cs₂ZrSe₃, would have a npO(C) ground-state structure type, and this material has an apM(C) type state that is 1 meV/f.u. higher in total energy. In this metastable structure, the angle β is 90° and lattice constants a and b are different from the calculated ground state by ≈ 0.08 Å. We hypothesize that the increased size and polarizability of X = Se when compared to combinations with X = O or S affords less structural rigidity and that further exploration of compositional tuning using chalcogenide anions to stabilize polar and antipolar structure types is warranted.

Eight of the compositions relax to a computed ground state of either the apM(C) or apO(P) type. Of this set, Na₂CS₃ and Tl_2CS_3 have an apM(C) ground state and apO(P) metastable states, and this is a consequence of the resistance to deformation of the CS₃ unit. K₂TiS₃ has both an apO(P) ground state and apM(C) metastable state, and they are only 5 meV/f.u. different in total energy. Experimental characterization of K₂TiS₃ reported an apM(C) structure type (with $\beta = 91.8^{\circ}$)⁸³ and not an apO(P) type ground state, suggesting that this is definitely a composition that should also be experimentally reinvestigated. Of the remainder of the set of seven, K₂SnO₃, K₂PbO₃, Rb₂PbO₃, K₂TiO₃, and K₂ZrO₃, each combination has a DFT-predicted apO(P) type ground state and a low-lying pO(C) type metastable state. The polarization (P) of each of these metastable states is along the c axis and has values of 0.15, 0.18, 0.14, 0.10, and 0.11 C/m2 for the five combinations, respectively. Each value of P for this set is close to that of BaTiO₃, and all ΔE are below 10 meV/f.u and therefore potentially accessible. These materials should be considered candidate AFEs, even if the low-lying polar state is the nonswitchable pO(C) type, as other polar states not considered here might be both energetically accessible and switchable. In addition, we propose that compositional tuning of these five materials, to create more low-lying switchable polar states, should be explored. This is supported by how close in energy the

npO(C) type is to each combination. Inspection of Tables S2 and S3 of the Supporting Information shows that the npO(C) type is only 61, 130, 50, and 37 meV/f.u. for K_2SnO_3 , K_2PbO_3 , Rb_2PbO_3 , and K_2ZrO_3 , respectively, above the computed ground state. These ΔE values are all below the 200 meV/f.u. threshold for switchability and all four materials could be considered candidate AFEs if the compositions are tuned to induce switchable polar distortions.

In general, we find that for combinations in which the ground state is the pO(C) type, then pO(P) and pM(C) types are widely disfavored metastable states, but ΔE does change with changes in the compositions. The structural energetics of the six combinations with a pO(C) ground state are plotted in Figure 4.

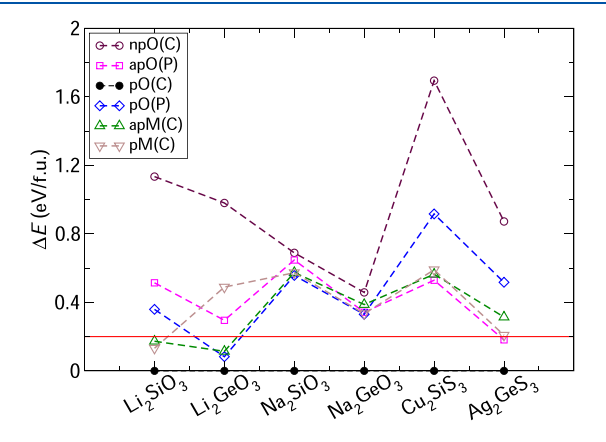


Figure 4. Shown here are the computed values of ΔE , relative to the pO(C) ground-state structure type, for all DFT-relaxed structures of Li₂SiO₃, Li₂GeO₃, Na₂SiO₃, Na₂GeO₃, Cu₂SiS₃, and Ag₂GeS₃. The red line is $\Delta E = 200$ meV/f.u., our cutoff for assessing whether a composition could be considered a proper ferroelectric.

For example, ΔE between pO(C) and pM(C) types for Li₂GeO₃ and Na₂GeO₃ is 0.489 and 0.334 eV, respectively, so adjusting the A-site did result in a 25% reduction in ΔE . The same is true of ΔE between pO(C) and npO(C) symmetries; the largest values are for Cu₂SiS₃ (1.694 eV), Li₂SiO₃ (1.134 eV), and Li₂GeO₃ (0.980 eV), which are combinations that contain smaller A- or B-sites than most of the family investigated here. In these combinations, there is a very large change in volume that accompanies differences in nonpolar and polar structure types, specifically in lattice constant a between npO(C) (and apO(P)in some cases) and pO(C) types. Table S1 of the Supporting Information shows that a of Na₂GeO₃ is 9.267 Å in the npO(C) type and 10.852 Å in the pO(C) type, precluding this a potential proper ferroelectric. Moreover, all ΔE values for the npO(C) type are above the 200 meV threshold to be considered as candidate proper ferroelectrics, as shown in Figure 4. While some apO(P) types are below or approaching this threshold, the drastic changes in coordination between apO(P) and pO(C) types also preclude most of this set from being considered potential proper ferroelectrics and antiferroelectrics; the six entries in Figure 4 are considered to be polar nonswitchable materials since $\Delta E > 200$ meV/f.u. and drastic changes in coordination and volume will prevent polarization switching. Thus far, our analysis has provided no proper FE from the set of 18 materials, only five candidate AFEs.

Focusing on the three A_2PbO_3 compositions, where A = K, Rb, and Cs, ΔE between the ground-state structure types and npO(C) types decreases an order of magnitude as the size of the A-site increases; the ΔE here are 130, 50, and 5 meV/f.u. for K, Rb, and Cs, respectively. K_2PbO_3 and Rb_2PbO_3 are two example combinations where structures initialized in the pO(P) type (and in one case the pM(C) type) relax to the higher-symmetry pO(C) type, indicating that polar modes may be stable under different conditions (epitaxial strain, changes in composition, etc. to tune the enthalpy of phase transitions) when B = Pb. Also

Table 2. Shown Here are the Total Irrep Amplitudes That Describe Each Structural Displacement Mode from the High-Symmetry npO(C) Type to Each of the Lower-Symmetry Structure Types apO(P), pO(C), pO(P), apM(C), and $pM(C)^a$

	apO(P)		pO(C)		pO(P)				apM(C)		pM(C)			
material	Γ^{1+}	Y ²⁻	Γ^{1+}	Γ^{2-}	Γ^{1+}	Γ^{2-}	Y ⁴⁺	Y ³⁻	Γ^{1+}	Γ^{4+}	Γ^{1+}	Γ^{4+}	Γ^{2-}	Γ^{3-}
Na ₂ CS ₃	_	-	1.18	2.64	-	-	-	_	0.79	2.18	2.01	1.88	1.05	1.64
Tl_2CS_3	2.79	2.66	3.69	3.59	_	_	_	_	0.68	1.98	1.49	1.92	1.18	3.96
Li_2SiO_3	1.81	2.44	3.65	4.63	0.50	0.01	2.12	2.18	2.06	2.02	0.44	0.39	1.50	0.71
Na ₂ SiO ₃	0.05	0.71	3.95	3.58	0.12	0.01	1.02	0.02	0.11	0.62	0.09	0.62	0.00	0.01
Li_2GeO_3	2.01	3.30	3.23	2.69	0.84	0.01	2.36	0.00	2.26	3.07	0.71	0.83	1.60	0.19
Na_2GeO_3	0.19	1.07	3.89	3.55	0.29	1.10	0.77	0.23	0.21	0.74	0.19	0.21	1.18	0.08
K_2SnO_3	0.08	0.97	4.45	4.11	0.09	1.10	0.01	0.02	0.06	0.52	0.09	0.01	1.11	0.03
K_2PbO_3	0.15	1.25	0.18	1.43	0.00	0.00	0.00	0.00	0.74	1.61	0.00	0.00	0.00	0.00
Rb_2PbO_3	0.07	0.98	0.08	1.13	0.00	0.00	0.00	0.00	0.01	0.35	0.08	0.00	1.14	0.01
Cs_2PbO_3	0.03	0.47	0.03	0.65	0.00	0.00	0.00	0.00	0.00	0.13	0.03	0.00	0.63	0.02
Cu_2SiS_3	1.38	2.76	2.99	2.86	1.92	3.06	1.92	1.56	1.44	2.58	1.56	1.33	2.05	0.45
Ag_2GeS_3	1.20	3.22	3.49	3.23	1.38	1.27	1.94	0.57	1.48	2.59	1.21	1.39	5.61	0.81
K_2TiO_3	0.01	0.45	0.00	0.18	0.00	0.00	0.00	0.00	0.00	0.00	0.00	0.00	0.00	0.00
K_2TiS_3	0.05	0.63	5.14	4.76	0.00	0.16	0.00	0.00	0.03	0.43	0.01	0.00	0.23	0.01
Cs_2TiS_3	0.00	0.00	0.00	0.00	0.00	0.00	0.00	0.00	0.00	0.00	0.00	0.00	0.00	0.00
K_2ZrO_3	0.07	0.92	4.46	3.93	0.07	1.04	0.01	0.02	0.02	0.03	0.07	0.01	1.05	0.03
Cs_2ZrO_3	0.00	0.00	0.00	0.00	0.00	0.00	0.00	0.00	0.00	0.00	0.00	0.00	0.00	0.00
Cs_2ZrSe_3	0.04	0.27	0.04	0.02	0.03	0.01	0.00	0.00	0.04	0.02	0.01	0.00	0.00	0.02

[&]quot;All irrep amplitude data tabulated here were generated using the ISODISTORT" tool available through the ISOTROPY software suite. A dash in the irrep amplitude (for Na_2CS_3 and Tl_2CS_3) indicates that the relaxation yielded a structure type different than those tabulated here, as discussed in the main text of the manuscript.

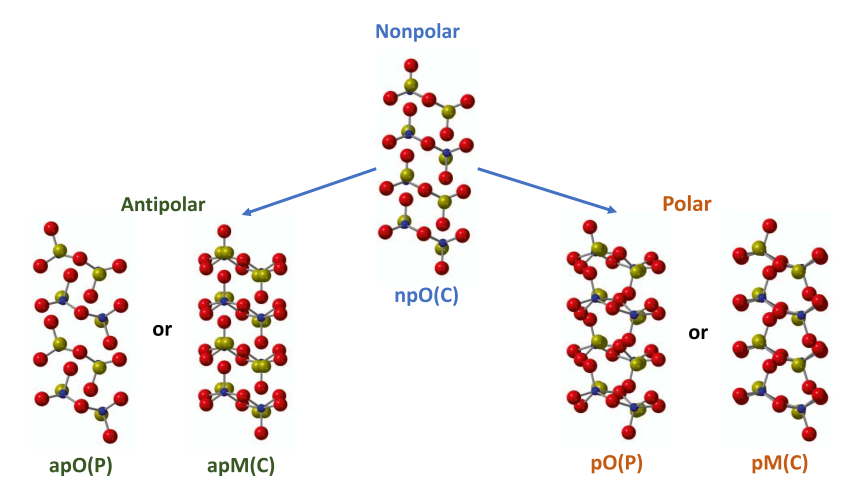


Figure 5. Stabilizing the displacement modes, from the high-symmetry nonpolar reference npO(C) structure type presented in Figure 2, via careful adjustment of compositional tuning or epitaxy is one route to create more structures with antipolar or polar ground states. Here, we show that are multiple orthorhombic and monoclinic structure types available to create new FEs and AFEs.

of note is that as the A-site changes from K to Rb to Cs, P of the (meta)stable structures also changes from 0.18 to 0.14 to 0.08 C/m^2 , consistent with the change in amplitude of Γ^{2-} in Table 2.

Table 2 is a collection of the displacement modes, in terms of irrep amplitudes from the npO(C) type, to each corresponding DFT-computed structure type. Analysis of the displacement mode amplitudes for the apO(P) type shows large amplitudes for A/B cation combinations that have either smaller A-sites (Li₂GeO₃), smaller B-sites (Cu₂SiS₃, Tl₂CS₃), or both smaller A and B-sites (Li₂SiO₃). These are compositions that were found in either apM(C) or pO(C) types in the ICSD. A few entries, K_2TiO_3 , Cs_2TiS_3 , and Cs_2ZrO_3 , show zero mode amplitude because these DFT calculations, initialized in the apO(P) type, relaxed to the higher-symmetry npO(C) type. This was a consistent observation throughout the study; compositions with smaller A- and B-sites tended to favor structures in apM(C) and pO(C) types, while compositions with a d^0 transition-metal B-site tended to favor npO(C) type.

The dashes appear in Table 2 for Na₂CS₃ and Tl₂CS₃ because they relaxed to structure types in higher symmetries than were initialized that were not part of our structure type set. When either composition was initialized in the pO(P) type, they relaxed to a structure type of *Pbcn* symmetry (space group 60) and Na_2CS_3 initialized in the apO(P) type relaxed to a structure type of *Imma* symmetry (space group 74). This is because polar and antipolar displacements of the 3-fold CS3 triangular unit in these structures are highly unfavored. Given the data presented here, neither of these materials is a likely candidate proper FE on their own; across all structure types, the CS₃ unit rarely showed any changes in bond length or relative orientation. One future route to explore for these two materials would be to create hybrid improper ferroelectrics via compositionally tuned variations of the A and B-site cations that would allow for switchable polarization via the trilinear coupling of one polar and two nonpolar irreps.

The largest mode amplitudes of the set belong to the Γ^{2-} irreps. They are consistently found in the pO(C) structure type and in the A_2BX_3 materials that contain B=Si or Ge, for which the pO(C) type is the experimentally determined and DFT-computed ground state. This trend is in agreement with the structural mode analysis presented in the previous section: in the phase transition from the npO(C) structure type, the edge-

sharing square-pyramidal BX_5 units would need to break and form multiple bonds to become corner-sharing BX_4 tetrahedra. The DFT-relaxed structures in the pO(C) type exhibited a very large increase in volume when compared to the npO(C) type, specifically from the increase in lattice constant a, as shown in Section S1 of the Supporting Information. This holds true when compared to other structure types in Table 2 and is correlated to the mode amplitudes of the Γ^{1+} irreps for materials with B=Si or Ga

If the polar mode described by the Γ^{2-} irrep is coupled to other modes, such as those described by the Y^{4+} and Y^{3-} irreps, and in the pO(P) type, or Γ^{4+} and Γ^{3-} in the pM(C) type, then the atomic displacements decrease in intensity and no longer disrupt the connectivity of the edge-sharing BX $_5$ units. In this sense, only structures from the pO(P) or pM(C) types could be examples of (im)proper ferroelectrics, since the polar displacement described by Γ^{2-} has been coupled to nonpolar displacement modes. The apM(C) type also includes large mode amplitudes for the combinations that contains B=Si or Ge for which there is a strong preference for 4-fold tetrahedral coordination. The pO(P) type was not found to be the ground state for any of the $18~A_2BX_3$ compositions investigated here and only one composition relaxed to a pM(C) ground state: Cs_2PbO_3 .

Analyzing the combined DFT and experiment structural and energetic data in its entirety, we can draw general conclusions about the structure-property relationships of the A₂¹⁺B⁴⁺X₃²⁻ family. Having the B-site cation as a C atom, like in the CS₃ unit, and having combinations of Li/Na with Si/Ge (most of the smaller ionic radii combinations) will lead to ground-state structure types in which edge-sharing BX₅ network is disrupted. Combinations with A = Rb or Cs tend to have fewer stable polar or antipolar displacement modes and will have ground states that are higher-symmetry orthorhombic structure types like the npO(C) (Cs₂ZrO₃, Cs₂ZrSe₃) or apO(P) types (Rb₂PbO₃). If instead we combine smaller A-sites and larger B-sites, as in Li₂PbO₃, 110 or increase the anion as well, as in Rb₂ZrTe₃, 111 then the coordination changes entirely and the resulting monoclinic structures can no longer be easily related to other members of the $A_2^{1+}B^{4+}X_3^{2-}$ set studied here. This limits our choices of A- and B-site combinations from the standpoint of compositional tuning to create new FEs and AFEs from the set

Table 3. Tabulated Here are the DFPT-Computed Properties of a Representative Sampling of the Known Members of the A₂BX₃ Family, Which are Categorized by Structure Type and DFT-Computed Ground-State Symmetry^a

type	symmetry	material	ϵ_{xx}	ϵ_{yy}	ϵ_{zz}	Z_{xx}^{B}	Z_{xz}^{B}	Z_{yy}^{B}	Z_{zx}^{B}	Z_{zz}^{B}
npO(C)	Стст	K_2TiO_3	2.90	3.12	3.61	2.38	0.00	2.94	0.00	5.18
		Cs_2ZrO_3	3.32	3.51	3.60	2.99	0.00	3.24	0.00	5.09
		Cs_2TiS_3	3.87	4.35	6.53	1.74	0.00	2.47	0.00	6.32
apO(P)	Pnma	K_2PbO_3	3.22	3.48	4.56	2.03	0.00	2.75	0.00	4.59
		Rb_2PbO_3	3.30	3.53	4.48	2.06	0.00	2.76	0.00	4.65
		K_2SnO_3	2.92	3.01	3.54	2.28	0.00	2.68	0.00	4.29
pO(C)	$Cmc2_1$	Li_2GeO_3	3.01	3.01	3.17	2.87	0.00	3.11	0.00	3.48
		Na ₂ SiO ₃	2.40	2.43	2.46	2.59	0.00	2.79	0.00	3.01
		Cu_2SiS_3	8.46	8.16	9.07	3.14	0.00	2.93	0.00	3.16
		Ag_2GeS_3	8.50	8.77	9.49	3.06	0.00	3.05	0.00	3.53
apM(C)	C2/c	Na_2CS_3	3.51	4.25	3.51	0.68	1.45	2.52	1.49	0.99

[&]quot;Presented first are the diagonal elements of the electronic contribution to the dielectric tensor (ϵ_{ii}) and then the components of the Born effective charge tensors of the B-sites.

of materials investigated in this work. Our choice of B-sites is ${\rm Ti}^{4+}$ (0.51 Å), ${\rm Sn}^{4+}$ (0.62 Å), ${\rm Zr}^{4+}$ (0.66 Å), and ${\rm Pb}^{4+}$ (0.73 Å), where the number in parentheses is the 5-fold coordinate ionic radii, and our choice of A-sites is ${\rm K}^{1+}$ (1.51 Å), ${\rm Tl}^{1+}$ (1.59 Å), and ${\rm Rb}^{1+}$ (1.61 Å), where the number in parentheses is the 8-fold coordinate ionic radii.

The known members of our set that fulfill this combination of A- and B-sites include K_2TiO_3 , K_2TiO_3 , K_2SnO_3 , K_2ZrO_3 , K_2PbO_3 , and Rb_2PbO_3 , all of which are computed to have an apO(P) ground state and/or a low-lying npO(C) state. These are the six combinations in which the addition of slightly smaller (or larger) cations can be added to create size mismatches that might be able to stabilize additional polar or antipolar ground-state structures in which ΔE can be adjusted further. Some examples of compositional tuning in this family would include adding Ag^{1+} on the A-site of K_2PbO_3 or Ti^{4+} to K_2SnO_3 to create polar materials from previously antipolar ground states. Another route would be to add Sn^{4+} to the B-site of nonpolar ground-state structures such as Cs_2TiS_3 and Cs_2ZrO_3 to create antipolar materials.

Figure 5 depicts some of the multiple structure types available to create new antipolar (apO(P), apM(C)) and polar (pO(P), apM(C))pM(C)) A_2BX_3 materials, assuming that the pO(C) structure type is not switchable and thus not a proper ferroelectric. To illustrate how one could use the data compiled here to create new proper ferroelectrics, we use Na₂GeO₃ as an example test case. Table 2 shows that one can induce continuous displacement modes between npO(C) and both pO(P) and pM(C)types. Table S1 of the Supporting Information shows that while the DFT-computed ground-state structure of Na₂GeO₃ is of pO(C) type, the ΔE between npO(C) and pO(P) and pM(C)types is 0.158 and 0.154 eV/f.u., respectively, well below the 200 meV threshold discussed in the Introduction. To investigate if these polar structure types can be switched to a state of opposite polarization, we need to induce displacements from the highsymmetry npO(C) type that are equal and opposite to the previously computed structures in pO(P) and pM(C) types. The resultant structures are then let fully relax to (locally) stable energetic minima, and then the Berry phase polarization of both sets of structures is computed. Calculations indicate that P, for these structures have values of 0.19 and -0.19 C/m^2 for the pO(P) type and values of 0.22 and -0.22 C/m² for the pM(C)type. This demonstrates that even for Na₂GeO₃, there exist metastable structures of opposite polarization with a barrier to switch that is less than that of BaTiO₃.

Finally, we present the DFPT-computed properties for a representative set of A2BX3 materials in Table 3, where the entries are categorized by their DFT-predicted ground state. The range of materials surveyed include only those in which the DFT-computed ground state matches the symmetry of the experimentally determined crystal structure. The values of ϵ_{ii} range of $\approx 2.5-4.5$, with the exception being the sulfides Cs_2TiS_3 , Cu_2SiS_3 , and Ag_2GeS_3 , where ϵ values of the two polar sulfides, that also contain a late d-block A-site, are more than double the other entries. Table 3 also shows that all values of Z_{xx}^{B} $Z_{vv}^{\rm B}$ and $Z_{xz}^{\rm B}$ are below the nominal charge of 4+ for the B-site, with many values at or below 2. The values of $Z_{77}^{\rm B}$ for entries with a ground-state symmetry of Cmcm and Pnma are above 4 and below 4 for entries with a ground-state symmetry of Cmc21 and C2/c. Since the Z_{zz}^{B} of the polar $Cmc2_{1}$ and antipolar C2/cground states is below the nominal valence charge, this may affect charge screening and decrease the depolarizing field of the thin films made with these materials. Recent work on polar intermetallic half-Heusler phases has posited that minimizing or modulating the depolarization field of a polar material, whether at a surface or interface, would be advantageous in the design of novel materials for energy generation and energy storage. 46,47 The A₂BX₃ family of materials presented here may yield an opportunity to investigate the same effects in polar and antipolar oxides and sulfides.

CONCLUSIONS

In this manuscript, we develop a procedure that combines crystallographic database mining and DFT calculations to explore the structure-property relationships of families of experimentally characterized oxide and chalcogenides whose FE and AFE properties may have previously gone overlooked. We use the ICSD to obtain crystallographic information for 18 compositions of chemical formula $A_2^{1+}B^{4+}X_3^{2-}$. These compositions have been assigned structure types, some of which had been referred to as related, but to the best of our knowledge, no symmetry relationships had previously been established. The space groups of the structure types of the compositions are subgroups of parent Cmcm symmetry and can therefore be related by continuous distortions. We use this information to assess potential second-order phase transitions between six different structure types, four known and two new. Using a combination of crystallographic data, ionic size, and displacive phase transition theory, we show why the known members of the Na₂SiO₃ structure type (pO(C) here) cannot be considered

proper ferroelectrics: inducing only the polar displacement modes described by the Γ^{2-} irrep causes a structural reorganization that prohibits FE switchability. We present an alternate method to design proper (and hybrid improper) FEs by coupling this mode to nonpolar or antipolar distortion modes. We explore this with two examples, the pO(P) and pM(C) structure types, which maintain the coordination of the edge-sharing BX_5 square pyramids, prevent the large changes in lattice constants and displacements that precluded ferroelectric switchability in the pO(C) type.

Comparison of the DFT-computed structures also leads to an informal set of design rules for mapping out which combinations may be excluded from preliminary experimental investigations. B-sites of smaller cations, such as C, Si, and Ge, lead to groundstate structures where the B-sites are 3- or 4-fold coordinate, and if the A-site is also small, like with Li, Na, and Cu, the resultant structures are too high in energy to switch or relax to nonpolar structures. We then go on to suggest that at least seven members of the A₂BX₃ family might be studied as is or adjusted to create new example FEs and AFEs. Of this set, the compositions that have a DFT-computed, and previously experimentally verified, apO(P) type ground state may already be antiferroelectric, and this functional property has previously gone overlooked. K₂SnO₃, K₂ZrO₃, K₂PbO₃, and Rb₂PbO₃ each have a polar metastable state within 10 meV/f.u. of their antipolar ground state, qualifying them as known oxides that might be candidate AFEs. With regards to compositional tuning, our investigation suggests that there are a few routes available to create new FEs and AFEs. The first would be to create polar/antipolar materials from compositions with nonpolar ground states (Cs₂TiS₃, Cs₂ZrO₃, Cs₂ZrSe₃) and the second would be to create polar materials from compositions with antipolar ground states (K₂PbO₃, Rb₂PbO₃). Compositional tuning has already been used to create polar monoclinic phases, ¹¹⁴ metastable ternary phases, ¹¹⁵ and solid electrolytes ¹¹⁶ from Na₂SiO₃ and Li₂SiO₃. Here, our goal would be to design systems in which the coordination of the BX₅ square pyramids of the structures is maintained while A-sites are free to displace in polar or antipolar patterns. Our study also suggests that the four combinations in which there are discrepancies between the DFT-relaxed groundstate structure and the structure reported in the ICSD (K₂TiO₃, K_2TiS_3 , Cs_2TiS_3 , Cs_2PbO_3) be experimentally reinvestigated, as they may also be materials in which the difference between the polar and antipolar/nonpolar states may be minimal. Lowtemperature diffraction experiments on these materials would complement prior structural determinations and the present work, illustrating if entropic effects are responsible for the multiple discrepancies in the ground-state structure.

The main goal of this study is to develop the structure—property relationships of a family of materials whose functional properties may have previously gone unmeasured and posit questions that could be answered via experiment, such as to the nature and extent of polarization switching and if the tunability of properties such as ΔE , ϵ , and Z^* could position the A_2BX_3 materials to be as well developed as the perovskites. This work is intended to complement recent studies where first-principles calculations have shown that theory can lead to experimental insights; for example, DFT has shown that the polar wurtzite structure can exhibit ferroelectricity via compositional tuning, 117,118 the existence of ferroelectric distortions in metals 36,119 such as $LiOsO_3^{120}$ and WTe_2^{121} and that two-dimensional (2D)-layered chalcogenides can contain multiple polarization states. 122,123 In this way, combining known structures from

crystallographic databases with first-principles calculations can lead to breakthroughs in the fields of energy generation and energy storage by mapping out potential phase transitions, optimizing stoichiometries, and prioritizing further investigations.

ASSOCIATED CONTENT

Supporting Information

The Supporting Information is available free of charge at https://pubs.acs.org/doi/10.1021/acs.jpcc.0c03093.

DFT-relaxed lattice parameters and corresponding ΔE , as well as crystallographic information with example Wyck-off parameters, a comparison between DFT-relaxed and experimentally determined lattice parameters, and a comparison between WC and PBE-GGA exchange-correlation functionals (PDF)

AUTHOR INFORMATION

Corresponding Author

Joseph W. Bennett — Department of Chemistry and Biochemistry, University of Maryland, Baltimore County, Baltimore, Maryland 21250, United States; ⊙ orcid.org/0000-0002-7971-4772; Email: bennettj@umbc.edu

Complete contact information is available at: https://pubs.acs.org/10.1021/acs.jpcc.0c03093

Notes

The author declares no competing financial interest.

ACKNOWLEDGMENTS

J.W.B. acknowledges the resources provided by the College of Natural and Mathematical Sciences and the Department of Chemistry and Biochemistry at the University of Maryland, Baltimore County. This work used the Extreme Science and Engineering Discovery Environment (XSEDE¹²⁴), which is supported by the National Science Foundation grant number ACI-1548562 through allocation ID TG-CHE190075. The hardware used in some of the computational studies is part of the UMBC High Performance Computing Facility (HPCF). The facility is supported by the U.S. National Science Foundation through the MRI program (grant nos. CNS-0821258, CNS-1228778, and OAC-1726023) and the SCREMS program (grant no. DMS-0821311), with additional substantial support from the University of Maryland, Baltimore County (UMBC).

REFERENCES

- (1) Zakutayev, A.; Zhang, X.; Nagaraja, A.; Yu, L.; Lany, S.; Mason, T. O.; Ginley, D. S.; Zunger, A. Theoretical Prediction and Experimental Realization of New Stable Inorganic Materials Using the Inverse Design Approach. *J. Am. Chem. Soc.* **2013**, *135*, 10048–10054.
- (2) Kalinin, S. V.; Sumpter, B. G.; Archibald, R. K. Big-Deep-Smart Data in Imaging for Guiding Materials Design. *Nat. Mater.* **2015**, *14*, 973–980.
- (3) Zunger, A. Inverse Design in Search of Materials with Target Functionalities. *Nat. Rev. Chem.* **2018**, *2*, No. 0121.
- (4) Alberi, K.; Nardelli, M. B.; Zakutayev, A.; Mitas, L.; Curtarolo, S.; Jain, A.; Fornari, M.; Marzari, N.; Takeuchi, I.; Green, M. L.; et al. The 2019 Materials by Design Roadmap. *J. Phys. D: Appl. Phys.* 2019, 52, No. 013001.
- (5) Wang, F.; Grinberg, I.; Rappe, A. M. Band Gap Engineering Strategy via Polarization Rotation in Perovskite Ferroelectrics. *Appl. Phys. Lett.* **2014**, *104*, No. 152903.

- (6) Filip, M. R.; Eperon, G. E.; Snaith, H. J.; Giustino, F. Steric Engineering of Metal-Halide Perovskites with Tunable Optical Band Gaps. *Nat. Commun.* **2014**, *5*, No. 5757.
- (7) D'Innocenzo, V.; Kandada, A. R. S.; Bastiani, M. D.; Gandini, M.; Petrozza, A. Tuning the Light Emission Properties by Band Gap Engineering in Hybrid Lead Halide Perovskite. *J. Am. Chem. Soc.* **2014**, 136, 17730–17733.
- (8) Walsh, A. Principles of Chemical Bonding and Band Gap Engineering in Hybrid Organic-Inorganic Halide Perovskites. *J. Phys. Chem. C* **2015**, *119*, 5755–5760.
- (9) Madsen, G. K. H. Automated Search for New Thermoelectric Materials: The Case of LiZnSb. *J. Am. Chem. Soc.* **2006**, *128*, 12140–12146.
- (10) Yan, J.; Gorai, P.; Ortiz, B.; Miller, S.; Barnett, S. A.; Mason, T.; Stevanovic, V.; Toberer, E. S. Material Descriptors for Predicting Thermoelectric Performance. *Energy Environ. Sci.* **2015**, *8*, 983–994.
- (11) Banik, A.; Roychowdhury, S.; Biswas, K. The Journey of Tin Chalcogenides Towards High-Performance Thermoelectrics and Topological Materials. *Chem. Commun.* **2018**, *54*, 6573–6590.
- (12) Roychowdhury, S.; Samanta, M.; Perumal, S.; Biswas, K. Germanium Chalcogenide Thermoelctrics: Electronic Structure Modulation and Low Lattice Thermal Conductivity. *Chem. Mater.* **2018**, *30*, 5799–5813.
- (13) Kamihara, Y.; Watanabe, T.; Hirano, M.; Hosono, H. Iron-Based Layered Superconductor La[$O_{1-x}F_x$]FeAs (x=0.05-0.12) with T_c = 26 K. *J. Am. Chem. Soc.* **2008**, *130*, 3296–3297.
- (14) Yakita, H.; Ogino, H.; Okada, T.; Yamamoto, A.; Kishio, K.; Tohei, T.; Ikuhara, Y.; Gotoh, Y.; Fujihisa, H.; Kataoka, K.; et al. A New Layered Iron Arsenide Superconductor:(Ca,Pr)FeAs₂. *J. Am. Chem. Soc.* **2014**, *136*, 846–849.
- (15) Bennett, J. W. Discovery and Design of Functional Materials: Integration of Database Searching and First-Principles Calculations. *Phys. Procedia* **2012**, *34*, 14–23.
- (16) Bennett, J. W.; Rabe, K. M. Integration of First-Principles Methods and Crystallographic Database Searches for New Ferroelectrics: Strategies and Explorations. *J. Solid State Chem.* **2012**, *195*, 21–31.
- (17) Garrity, K. F. High-throughput First-Principles Search for New Ferroelectrics. *Phys. Rev. B* **2018**, *97*, No. 024115.
- (18) Belsky, A.; Hellenbrandt, M.; Karen, V. L.; Luksch, P. New Developments in the Inorganic Crystal Structure Database (ICSD): Accessibility in Support of Materials Research and Design. *Acta Crystallogr., Sect. B: Struct. Sci.* **2002**, *58*, 364–369.
- (19) Hohenberg, P.; Kohn, W. Inhomogeneous Electron Gas. *Phys. Rev.* **1964**, *136*, B864–B871.
- (20) Kohn, W.; Sham, L. J. Self-Consistent Equations Including Exchange and Correlation Effects. *Phys. Rev.* **1965**, *140*, A1133–A1138.
- (21) Balachandran, P. V.; Puggioni, D.; Rondinelli, J. M. Crystal-Chemistry Guidelines for Noncentrosymmetric A_2BO_4 Ruddlesden-Popper Oxides. *Inorg. Chem.* **2014**, *53*, 336–348.
- (22) Rondinelli, J. M.; Fennie, C. J. Octahedral Rotation-Induced Ferroelectricity in Cation Ordered Perovskites. *Adv. Mater.* **2012**, *24*, 1961–1968.
- (23) Zhang, X.; Yu, L.; Zakutayev, A.; Zunger, A. Sorting Stable versus Unstable Hypothetical Compounds: The Case of Multi-Functional *ABX* Half-Heusler Filled Tetrahedral Structures. *Adv. Funct. Mater.* **2012**, 22, 1425–1435.
- (24) Yu, L.; Zunger, A. Identification of Potential Photovoltaic Absorbers Based on First-Principles Spectroscopic Screening of Materials. *Phys. Rev. Lett.* **2012**, *108*, No. 068701.
- (25) Yu, L.; Kokenyesi, R. S.; Kaszler, D. A.; Zunger, A. Inverse Design of High Absorption Thin-Film Photovoltaic Materials. *Adv. Energy Mater.* **2013**, *3*, 43–48.
- (26) Yan, F.; Zhang, X.; Yu, Y. G.; Yu, L.; Nagaraja, A.; Mason, T. O.; Zunger, A. Design and Discovery of a Novel half-Heusler Transparent Hole Conductor Made of All-Metallic Heavy Elements. *Nat. Commun.* **2015**, No. 7308.
- (27) Gautier, R.; Zhang, X.; Hu, L.; Yu, L.; Lin, Y.; Sunde, T. O. L.; Chon, D.; Poeppelmeier, K. R.; Zunger, A. Prediction and Accelerated

- Laboratory Discovery of Previously Unknown 18-electron *ABX* Compounds. *Nat. Chem.* **2015**, *7*, 308–316.
- (28) Jain, A.; Hautier, G.; Moore, C. J.; Ong, S. P.; Fischer, C. C.; Mueller, T.; Persson, K. A.; Ceder, G. A High-Throughput Infrastructure for Density Functional Theory Calculations. *Comput. Mater. Sci.* **2011**, *50*, 2295–2310.
- (29) Hautier, G.; Jain, A.; Ong, S. P.; Kang, B.; Moore, C.; Doe, R.; Ceder, G. Phosphates as Lithium-Ion Battery Cathodes: An Evaluation Based on High-throughput *ab initio* Calculations. *Chem. Mater.* **2011**, 23, 3495–3508.
- (30) Hautier, G.; Jain, A.; Chen, H.; Moore, C.; Ong, S. P.; Ceder, G. Novel Mixed Polyanions Lithium-Ion Battery Cathode Materials Predicted by High-Throughput *ab initio* Calculations. *J. Mater. Chem.* **2011**, *21*, 17147–17153.
- (31) Lee, J. H.; Fang, L.; Vlahos, E.; Ke, X.; Jung, Y. W.; Kourkoutis, L. F.; Kim, J.-W.; Ryan, P. J.; Heeg, T.; Roeckerath, M.; et al. A Strong Ferroelectric Ferromagnet Created by Means of Spin-Lattice Coupling. *Nature* **2010**, *466*, 954–958.
- (32) Benedek, N. A.; Fennie, C. J. Hybrid Improper Ferroelectricity: A Mechanism for Controllable Polarization-Magnetization Coupling. *Phys. Rev. Lett.* **2011**, *106*, No. 107204.
- (33) Rondinelli, J. M.; May, S. J.; Freeland, J. W. Control of Octahedral Connectivity in Perovskite Oxide Heterostructures: An Emerging Route to Multifunctional Materials Discovery. *MRS Bull.* **2012**, *37*, 261–270.
- (34) Stroppa, A.; Barone, P.; Jain, P.; Perez-Mato, J. M.; Picozzi, S. Hybrid Improper Ferroelectricity in a Multiferroic and Magnetoelectric Metal-Organic Framework. *Adv. Mater.* **2013**, *25*, 2284–2290.
- (35) Kim, T. H.; Puggioni, D.; Yuan, Y.; Xie, L.; Zhou, H.; Campbell, N.; Ryan, P.J.; Choi, Y.; Kim, J.-W.; Patzner, J. R.; et al. Polar Metals by Geometric Design. *Nature* **2016**, *533*, 68–72.
- (36) Benedek, N. A.; Birol, T. Ferroelectric Metals Reexamined: Fundamental Mechansisms and Design Considerations for New Materials. *J. Mater. Chem. C* **2016**, *4*, 4000–4015.
- (37) Zhang, R.; Abbett, B. M.; Read, G.; Lang, F.; Lancaster, T.; Tran, T. T.; Halasyamani, P. S.; Blundell, S. J.; Benedek, N. A.; Hayward, M. A. La₂SrCr₂O₇: Controlling the Tilting Distortions of *n*=2 Ruddlesden-Popper Phases through A-site Cation Disorder. *Inorg. Chem.* **2016**, *55*, 8951–8960.
- (38) Zhou, X.; Rodriguez, E. E. Tetrahedral Transition Metal Chalcogenides as Functional Inorganic Materials. *Chem. Mater.* **2017**, 29, 5737–5752.
- (39) Young, J.; Moon, E.-J.; Mukherjee, D.; Stone, G.; Gopalan, V.; Alem, N.; May, S. J.; Rondinelli, J. M. Polar Oxides without Inversion Symmetry through Vacancy and Chemical Order. *J. Am. Chem. Soc.* **2017**, *139*, 2833–2841.
- (40) Zhu, T.; Khalsa, G.; Havas, D. M.; Gibbs, A. S.; Zhang, W.; Halasyamani, P. S.; Benedek, N. A.; Hayward, M. A. Cation Exchange as a Mechanism to Engineer Polarity in Layered Perovskites. *Chem. Mater.* **2018**, *30*, 8915–8924.
- (41) Allmann, R.; Hinek, R. The Introduction of Structure Types into the Inorganic Crystal Structure Database ICSD. *Acta Crystallogr., Sect. A: Found. Crystallogr.* **2007**, *A*63, 412–417.
- (42) Halasyamani, P. S.; Poeppelmeier, K. R. Noncentrosymmetric Oxides. *Chem. Mater.* **1998**, *10*, 2753–2769.
- (43) Bennett, J. W. Surveying Polar Materials in the Inorganic Crystal Structure Database to Identify Emerging Structure Types. *J. Solid State Chem.* **2020**, *281*, No. 121045.
- (44) Roy, A.; Bennett, J. W.; Rabe, K. M.; Vanderbilt, D. Half-Heusler Semiconductors as Piezoelectrics. *Phys. Rev. Lett.* **2012**, *109*, No. 037602.
- (45) Bennett, J. W.; Garrity, K. F.; Rabe, K. M.; Vanderbilt, D. Hexagonal *ABC* Semiconductors as Ferroelectrics. *Phys. Rev. Lett.* **2012**, 109. No. 167602.
- (46) Garrity, K. F.; Rabe, K. M.; Vanderbilt, D. Hyperferroelectrics: Proper Ferroelectrics with Persistent Polarization. *Phys. Rev. Lett.* **2014**, *112*, No. 127601.
- (47) Kawasaki, J. K. Heusler Interfaces: Opportunities Beyond Spintronics. APL Mater. 2019, 7, No. 080907.

- (48) Bennett, J. W.; Garrity, K. F.; Rabe, K. M.; Vanderbilt, D. Orthorhombic *ABC* Semiconductors as Antiferroelectrics. *Phys. Rev. Lett.* **2013**, *110*, No. 017603.
- (49) Choi, T.; Lee, S.; Choi, Y. J.; Kiryukhin, V.; Cheong, S.-W. Switchable Ferroelectric Diode and Photovoltaic Effect in BiFeO₃. *Nature* **2009**, 324, 63–66.
- (50) Yang, S. Y.; Seidel, J.; Byrnes, S. J.; Shafer, P.; Yang, C.-H.; Rossell, M. D.; Yu, P.; Chu, Y.-H.; Scott, J. F.; Ager, J. W.; et al. Above-Bandgap Voltages from Ferroelectric Photovoltaic Devices. *Nat. Nanotechnol.* **2010**, *5*, 143–147.
- (51) Butler, K. T.; Frost, J. M.; Walsh, A. Ferroelectric Materias for Solar Energy Conversion: Photoferroics Revisited. *Energy Environ. Sci.* **2015**. *8*, 838–848.
- (52) Tan, L. Z.; Zheng, F.; Young, S. M.; Wang, F.; Liu, S.; Rappe, A. M. Shift Current Bulk Photovoltaic Effect in Polar Materials: Hybrid and Oxide Perovskites and Beyond. *npj Comput. Mater.* **2016**, 2, No. 16026.
- (53) Cook, A. M.; Fregoso, B. M.; de Juan, F.; Coh, S.; Moore, J. E. Design Principles for Shift Current Photovoltaics. *Nat. Commun.* **2017**, *8*, No. 14176.
- (54) Nakamura, M.; Horiuchi, S.; Kagawa, F.; Ogawa, N.; Kurumaji, T.; Tokura, Y.; Kawasaki, M. Shift Current Photovoltaic Effect in a Ferroelectric Charge-Transfer Complex. *Nat. Commun.* **2017**, 8, No. 281.
- (55) Cohen, R. E. Origin of Ferroelectricity in Perovskite Oxides. *Nature* **1992**, 358, 136–138.
- (56) Ghosez, P.; Cockayne, E.; Waghmare, U. V.; Rabe, K. M. Lattice Dynamics of BaTiO₃, PbTiO₃, and PbZrO₃: A Comparative First-Principles Study. *Phys. Rev. B* **1999**, *60*, 836–843.
- (57) Bousquet, E.; Dawber, M.; Stucki, N.; Lichtensteiger, C.; Hermet, P.; Garliglio, S.; Triscone, J.-M.; Ghosez, P. Improper Ferroelectricity in Perovskite Oxide Artifical Superlattices. *Nature* **2008**, 452, 732–737.
- (58) Benedek, N. A.; Mulder, A. T.; Fennie, C. J. Polar Octahedral Rotations: A Path to New Multifunctional Materials. *J. Solid State Chem.* **2012**, *195*, 11–20.
- (59) Rabe, K. M. Antiferroelectricity in Oxides: A Reexamination; Wiley, 2013; pp 221–244.
- (60) Reyes-Lillo, S. E.; Garrity, K. F.; Rabe, K. M. Antiferroelectricity in Thin-Film ZrO₂ from First-Principles. *Phys. Rev. B.* **2014**, *90*, No. 140103.
- (61) Mishra, R.; Ali, M.; Bharadwaj, S. R.; Das, D. Preparation of Cs_2ZrO_3 and Cs_2ThO_3 Through Sol-Gel Method and Their Characterization. *J. Therm. Anal. Calorim.* **2001**, *66*, 779–784.
- (62) Khalsa, H. S.; Smith, M. D.; zur Loye, H.-C. Crystal Growth and Structure Determination of K₂TiO₃: A Five Coordinate Titanate. *Mater. Res. Bull.* **2009**, *44*, 91–94.
- (63) Beck, J.; Benz, S. The Crystal Structure of Thallium(I) Trithiocarbonate, Tl₂CS₃. Z. Anorg. Allg. Chem. **2009**, 635, 962–965.
- (64) Masubuchi, Y.; Miyazaki, R.; Kirkuchi, H.; Motohashi, T.; Kikkawa, S. Exfoliation of One-Dimensional TiO₅ Chain in K₂TiO₃. *Dalton Trans.* **2014**, *43*, 13751–13755.
- (65) Terry, R. J.; McMillen, C. D.; Chen, X.; Wen, Y.; Zhu, L.; Chumanov, G.; Kolis, J. W. Hydrothermal Single Crystal Growth and Second Harmonic Generation of Li₂SiO₃, Li₂GeO₃, and Li₂Si₂O₅. *J. Cryst. Growth* **2018**, 493, 58–64.
- (66) Panek, P.; Hoppe, R. Zur Kristallstruktur von Cs₂PbO₃. Z. Anorg. Allg. Chem. **1972**, 393, 13–22.
- (67) Stoll, H.; Hoppe, R. Ueber K₂PbO₃, Rb₂PbO₃ und Cs₂PbO₃. Z. Anorg. Allg. Chem. **1987**, 551, 151–162.
- (68) Kroumova, E.; Perez-Mato, J. M.; Aroyo, M. I. WYCKSPLIT: A Computer Program for Determination of the Relations of Wyckoff Positions for a Group-Subgroup Pair. J. Appl. Crystallogr. 1998, 31, 646.
- (69) Aroyo, M. I.; Perez-Mato, J. M.; Capillas, C.; Kroumova, E.; Ivantchev, S.; Madariaga, G.; Kirov, A.; Wondratschek, H. Bilbao Crystallographic Server I: Databases and Crystallographic Computing Programs. Z. Kristallogr. 2006, 221, 15–27.
- (70) Aroyo, M. I., Kirov, A.; Capillas, C.; Perez-Mato, J. M.; Wondratschek, H. Bilbao Crystallographic Server II: Representations of

- Crystallographic Point Groups and Space Groups. Acta Crystallogr., Sect. A: Found. Crystallogr. 2006, 62, 115–128.
- (71) Campbell, B. J.; Stokes, H. T.; Tanner, D. E.; Hatch, D. M. ISODISPLACE: AWeb-Based Tool for Exploring Structural Distortions. J. Appl. Crystallogr. 2006, 39, 607–614.
- (72) Stokes, H. T.; Hatch, D. M.; Campbell, B. J. ISOTROPY Software Suite. http://iso.byu.edu.
- (73) Sani, A.; Hanfland, M.; Levy, D. Pressure and Temperature Dependence of the Ferroelectric-Paraelectric Phase Transition in PbTiO₃. *J. Solid State Chem.* **2002**, *167*, 446–452.
- (74) Wang, Y. G.; Zhong, W. L.; Zhang, P. L. Surface Effects and Size Effects on Ferroelectrics With a First-Order Phase Transition. *Phys. Rev.* B **1996**, 53, 11439.
- (75) Jain, P.; Ramachandran, V.; Clark, R. J.; Zhou, H. D.; Toby, B. H.; Dalal, N. S.; Kroto, H. W.; Cheetham, A. K. Multiferroic Behavior Associated with an Order-Disorder Hydrogen Bonding Transition in Metal-Organic Frameworks (MOFs) with the Perovskite *ABX*₃ Architecture. *J. Am. Chem. Soc.* **2009**, *131*, 13625–13627.
- (76) Benedek, N. A.; Rondinelli, J. M.; Djani, N.; Ghosez, P.; Lightfoot, P. Understanding Ferroelectricity in Layered Perovskites: New Ideas and Insights From Theory and Experiments. *Dalton Trans.* **2015**, *44*, 10543–10558.
- (77) Yoshida, S.; Akamatsu, H.; Tsuji, R.; Hernandez, O.; Padmanabhan, H.; Gupta, A. S.; Gibbs, A. S.; Mibu, K.; Murai, S.; Rondinelli, J. M.; et al. Hybrid Improper Ferroelectricity in (Sr,Ca)₃Sn₂O₇ and Beyond: Universal Relationship Between Ferroelectric Transition Temperature and Tolerance Factor in n=2 Ruddlesden-Popper Phases. *J. Am. Chem. Soc.* **2018**, *140*, 15690–15700.
- (78) Nowadnick, E. A.; Fennie, C. J. Domains and Ferroelectric Switching Pathways in Ca₃Ti₂O₇ from First-Principles. *Phys. Rev. B* **2016**, *94*, No. 104105.
- (79) Hoppe, R.; Roehrborn, H. J.; Walker, H. Neue Plumbate und Stannate der Alkalimetalle. *Naturwissenschaften* **1964**, *51*, 86.
- (80) Hoppe, R.; Stover, H. D. Zur Kristallstruktur von Rb₂PbO₃. Z. Anorg. Allg. Chem. **1977**, 437, 123–126.
- (81) Seeger, K.; Hoppe, R. Die Kristallstruktur von Rb₂PbO₃. Z. Anorg. Allg. Chem. **1970**, 375, 255–263.
- (82) Henseler, U.; Jansen, M. Modifizierte Darstellung und Kristallstrukturbestimmung von β -Na₂CS₃. Z. Anorg. Allg. Chem. **1993**, 619, 1203–1208.
- (83) Klepp, K. O. K. K₂TiS₃, ein neues Thiotitanat(IV) mit funffach koordiniertem Titan. *Z. Naturforsch. B* **1992**, 47, 201–204.
- (84) Bhalla, A. S.; Cross, L. E.; Newham, R. E. Polar Twins in Lithium Metasilicate and Metagermanate (Li₂SiO₃, Li₂GeO₃) Single Crystals. *J. Cryst. Growth* **1979**, *46*, 262–264.
- (85) Haussühl, S.; Liebertz, J.; Stahr, S. Single Crystal Growth and Pyreoelectric, Dielectric, Piezoelectric, Elastic, and Thermoelastic Properties of Orthorhombic Li₂SiO₃, Li₂GeO₃, and Na₂GeO₃. *Cryst. Res. Technol.* **1982**, *17*, 521–526.
- (86) Yu, Y. S.; Prabhu, S. S.; Perkowitz, S.; Kim, S. C. New Vibrational Modes in Single Crystal Li, GeO₃. Ferroelectrics **1998**, 205, 159–165.
- (87) Rahman, M. M.; Sultana, I.; Yang, T.; Chen, Z.; Sharma, N.; Glushenkov, A. M.; Chen, Y. Lithium Germanate (Li₂GeO₃): A High-Performance Anode Material for Lithium-Ion Batteries. *Angew. Chem.* **2016**, *128*, 16293–16297.
- (88) Gonze, X.; Amadon, B.; Anglade, P.-M.; Beuken, J.-M.; Bottin, F.; Boulanger, P.; Bruneval, F.; Caliste, D.; Caracas, R.; Cote, M.; et al. ABINIT: First-principles Approach to Material and Nanosystem Properties. *Comput. Phys. Commun.* **2009**, *180*, 2582–2615.
- (89) Gonze, X.; Jollet, F.; Abreu-Araujo, F.; Adams, D.; Amadon, B.; Applencourt, T.; Audouze, C.; Beuken, J.-M.; Bieder, J.; Bokhanchuk, A.; et al. Recent Developments in the ABINIT Software Package. *Comput. Phys. Commun.* **2016**, 205, 106–131.
- (90) Hamann, D. R.; Schlüter, M.; Chiang, C. Norm-Conserving Pseudopotentials. *Phys. Rev. Lett.* **1979**, 43, 1494–1497.
- (91) Vanderbilt, D. Soft Self-Consistent Pseudopotentials in a Generalized Eigenvalue Formalism. *Phys. Rev. B* **1990**, *41*, 7892–7895.

- (92) Hamann, D. R. Optimized Norm-Conserving Vanderbilt Pseudopotentials. *Phys. Rev. B* **2013**, 88, No. 085117.
- (93) Monkhorst, H. J.; Pack, J. D. Special Points for Brillouin-Zone Integrations. *Phys. Rev. B* **1976**, *13*, 5188–5192.
- (94) Gonze, X.; Lee, C. Dynamical Matrices, Born Effective Charges, Dielectric Permittivity Tensors, and Interatomic Force Constants from Density-Functional Perturbation Theory. *Phys. Rev. B* **1997**, 55, 10355–10368.
- (95) Baroni, S.; de Gironcoli, S.; Corso, A. D.; Giannozzi, P. Phonons and Related Crystal Properties from Density-Functional Perturbation Theory. *Rev. Mod. Phys.* **2001**, *73*, 515–562.
- (96) King-Smith, R. D.; Vanderbilt, D. Theory of Polarization of Crystalline Solids. *Phys. Rev. B* **1993**, *47*, 1651–1654.
- (97) Resta, R. Macroscopic Polarization in Crystalline Dielectrics: the Geometric Phase Approach. *Rev. Mod. Phys.* **1994**, *66*, 899–915.
- (98) Perdew, J. P.; Burke, K.; Ernzerhof, M. Generalized Gradient Approximation Made Simple. *Phys. Rev. Lett.* **1996**, *77*, 3865–3868.
- (99) Wu, Z.; Cohen, R. E. More Accurate Generalized Gradient Approximation for Solids. *Phys. Rev. B.* **2006**, 73, No. 235116.
- (100) Tran, F.; Laskowski, R.; Blaha, P.; Schwarz, K. Performance on Molecules, Surfaces, and Solids of the Wu-Cohen GGA Exchange-Correlation Energy Functional. *Phys. Rev. B* **2007**, *75*, No. 115131.
- (101) Ganesh, P.; Cohen, R. E. Pressure Induced Phase Transitions in PbTiO₃. *J. Phys.: Condens. Matter* **2009**, *21*, No. 064225.
- (102) Paul, A.; Sun, J.; Perdew, J. P.; Waghmare, U. V. Accuracy of First-Principles Interatomic Interactions and Predictions of Ferroelectric Phase Transitions in Perovskite Oxides: Energy Functional and Effective Hamiltonian. *Phys. Rev. B* **2017**, *95*, No. 054111.
- (103) Klepp, K. O.; Kolb, A. Crystal Structure of Dicaesium Triselenozirconate(IV) Cs₂ZrSe₃. Z. Kristallogr. 1998, 213, 694.
- (104) Harrison, M. R.; Francesconi, M. G. Mixed-Metal One-Dimensional Sulfides: A Class of Materials with Differences and Similarities to Oxides. *Coord. Chem. Rev.* **2011**, 255, 451–458.
- (105) Kerman, S.; Campbell, B. J.; Satyavarapu, K. K.; Stokes, H. T.; Perselli, F.; Evans, J. S. O. The Superstructure Determination of Displacive Distortions via Symmetry-Mode Analysis. *Acta Crystallogr.* Sect. A: Found. Crystallogr. 2012, 68, 222–234.
- (106) Stokes, H. T.; van Orden, S.; Campbell, B. J. ISOSUBGROUP: An Internet Tool for Generating Isotropy Subgroups of Crystallographic Space Groups. *J. Appl. Crystallogr.* **2016**, *49*, 1849–1853.
- (107) Rad, H. D.; Hoppe, R. Ueber Thiotitanate(IV): Synthese und Struktur von Cs, TiS, Z. Naturforsch. B 1978, 33, 1184–1185.
- (108) Sun, J.; Ruzsinszky, A.; Perdew, J. P. Strongly Constrained and Appropriately Normed Semilocal Density Functional. *Phys. Rev. Lett.* **2015**, *115*, No. 036402.
- (109) Zhang, Y.; Kitchaev, D. A.; Yang, J.; Chen, T.; Dacek, S. T.; Sarmiento-Perez, R. A.; Marques, M. A. L.; Peng, H.; Ceder, G.; Perdew, J. P.; et al. Efficient First-Principles Prediction of Solid Stability: Towards Chemical Accuracy. *npj Comput. Mater.* **2018**, *4*, No. 9.
- (110) Brazel, B.; Hoppe, R. Uber Oxoplumbate(IV) Die Kristallstruktur von HT-Li₂PbO₃. Z. Naturforsch. B **1983**, 38, 661–664.
- (111) Klepp, K. O.; Kolb, A. Komplexe Chalkogenide der IVa Metalle mit niedrigdimensionalen anionischen Partialstrukturen: Darstellung und Kristallstruktur von K₂ZrTe₃ und Rb₂ZrTe₃. Z. Naturforsch. B **1999**, 54, 441–446.
- (112) Shannon, R. D.; Prewitt, C. T. Revised Values of Effective Ionic Radii. *Acta Crystallogr., Sect. B: Struct. Crystallogr. Cryst. Chem.* **1970**, 26, 1046–1048.
- (113) Shannon, R. D. Revised Effective Ionic Radii and Systematic Studies of Interatomic Distances in Halides and Chalcogenides. *Acta Crystallogr., Sect. A* **1976**, *32*, 751–767.
- (114) West, A. R. Phase Equilibria in the System Na₂SiO₃-Li₂SiO₃. *J. Am. Ceram. Soc.* **1976**, *59*, 118–121.
- (115) West, A. R. Phase Equilibria in the System Na₂SiO₃-Li₂SiO₃-SiO₂. *J. Am. Ceram. Soc.* **1976**, *59*, 124–127.
- (116) Zulueta, Y. A.; Nguyen, M. T.; Dawson, J. A. Na- and K-Doped Li₂SiO₃ as an Alternative Solid Electrolyte for Solid State Lithium Batteries. *J. Phys. Chem. C* **2020**, 124, 4982–4988.

- (117) Zhang, S.; Fu, W. Y.; Holec, D.; Humphreys, C. J.; Moram, M. A. Elastic Constants and Critical Thicknesses of ScGaN and ScAlN. *J. Appl. Phys.* **2013**, *114*, No. 243516.
- (118) Fichtner, S.; Wolff, N.; Lofink, F.; Kienle, L.; Wagner, B. AlScN: A III-V Semiconductor Based Ferroelectric. *J. Appl. Phys.* **2019**, *125*, No. 114103.
- (119) Anderson, P. W.; Blount, E. I. Symmetry Considerations on Martensitic Transformations: "Ferroelectric" Metals? *Phys. Rev. Lett.* **1965**, *14*, 217–219.
- (120) Shi, Y.; Guo, Y.; Wang, X.; Princep, A. J.; Khalyavin, D.; Manuel, P.; Michiue, Y.; Sato, A.; Tsuda, K.; Yu, S.; et al. A Ferroelectric-Like Structural Transition in a Metal. *Nat. Mater.* **2013**, *12*, 1024–1027.
- (121) Fei, Z.; Zhao, W.; Palomaki, T. A.; Sun, B.; Miller, M. K.; Zhao, Z.; Yan, J.; Xu, X.; Cobden, D. H. Ferroelectric Switching of a Two-Dimensional Metal. *Nature* **2018**, *560*, 336–339.
- (122) Neumayer, S. M.; Eliseev, E. A.; Susner, M. A.; Tselev, A.; Rodriguez, B. J.; Brehm, J. A.; Pantelides, S. T.; Panchapakesan, G.; Jesse, S.; Kalinin, S. V.; et al. Giant Negative Electrostriction and Dielectric Tunability in a van der Waals Layered Ferroelectric. *Phys. Rev. Mater.* **2019**, 3, No. 024401.
- (123) Brehm, J. A.; Neumayer, S. M.; Tao, L.; O'Hara, A.; Chyasnavichus, M.; Susner, M. A.; McGuire, M. A.; Kalinin, S. V.; Jesse, S.; Ganesh, P.; et al. Tunable Quadruple-Well Ferroelectric van der Waals Crystals. *Nat. Mater.* **2020**, *19*, 43–48.
- (124) Towns, J.; Cockerill, T.; Dahan, M.; Foster, I.; Gaither, K.; Grimshaw, A.; Hazlewood, V.; Lanthrop, S.; Lifka, D.; Peterson, G. D.; et al. XSEDE:Accelerating Scientific Discovery. *Comput. Sci. Eng.* **2014**, *16*, 62–74.